Progressive Atmospheric Correction of Satellite Ocean-Color Imagery

Robert Frouin[a], Lydwine Gross[a], Bruno Pelletier[c]
[a]Scripps Institution of Oceanography, 8810 La Jolla Shores Drive, La Jolla, California
[b]Capgemini, 8 Rue Paul Mesplé, B. P. 1155, 31036 Toulouse, France
[c]Institut de Mathématiques et de Modélisation de Montpellier, UMR CNRS 5149,
Université de Montpellier II, Place Eugène bataillon, 34095 Montpellier, France

ABSTRACT

A methodology is proposed to correct satellite ocean-color imagery for the perturbing effects of the atmosphere and surface progressively, starting from the near infrared and advancing to the visible. First, a set of spectral bands is selected in the near infrared, for which the water body can be considered black, except in one of the spectral bands. The top-of-atmosphere reflectance in the selected bands, after correction for molecular scattering and sun glint contributions, is linearly combined to retrieve the ocean signal in the spectral band where the water body is not black. The coefficients of the linear combination minimize the perturbing effects, which are due to scattering and absorption by aerosols, and reflection by the surface. These effects are decomposed into principal components in the modeling. Second, other sets of spectral bands are selected, that progressively include shorter wavelengths. At each step, only the marine signal in one spectral band is unknown and therefore estimated. The methodology is developed for the Sea-viewing Wide Field-of-view Sensor (SeaWiFS), but is generally applicable to ocean-color sensors that measure in the visible and near infrared. Without measurements above one micrometer, however, the atmospheric correction is only accurate over Case-1 waters. Theoretical performance is evaluated from radiation-transfer simulations for a wide range of geophysical and angular conditions, including absorbing aerosols. Only Case-1 waters are considered in the simulations. The perturbing influence of the atmosphere and surface is minimized adequately for each set of wavelengths, except when the aerosol loading is large. The residual effects in the linear combination exhibit a bias of magnitude increasing with aerosol optical thickness. The bias can be reduced globally, by taking into account all the eigenvectors of the decomposition in principal components, not only the most significant ones. Errors in the estimated marine signal increase with decreasing wavelength (the residual effects at longer wavelengths propagate) and with increasing aerosol optical thickness. They become unacceptable when the aerosol optical thickness at 550 nm is above 0.3. Performance can be improved by optimizing the sets of selected wavelengths, or by using aerosol optical thickness estimated from the satellite data.

Key words: Ocean color, remote sensing, aerosols, and atmospheric correction

1. INTRODUCTION

Standard algorithms to estimate the concentration of marine constituents (e.g., chlorophyll-a concentration) from space[1-7] aim at correcting accurately atmosphere and surface effects on the measured top-of-atmosphere radiance. The procedure consists of estimating the aerosol radiance in the red and near infrared where the ocean can be considered black (i.e., totally absorbing), and extrapolating the estimated radiance to shorter wavelengths. The retrieved water-leaving radiance is then related to chlorophyll-a concentration or other variables using bio-optical models. This approach has been successful, and it is employed in the operational processing of data from major satellite ocean-color missions. In other

Remote Sensing of the Marine Environment, edited by Robert J. Frouin, Vijay K. Agarwal,
Hiroshi Kawamura, Shailesh Nayak, Delu Pan, Proc. of SPIE Vol. 6406, 64061S, (2006)
0277-786X/06/$15 · doi: 10.1117/12.698045

algorithms[8-13] aerosol properties and pigment concentration are determined in a single step. Through systematic variation of candidate aerosol models, phytoplankton scattering, pigment concentration, and aerosol optical thickness, a best fit to the spectral top-of-atmosphere radiance (visible and near infrared) is obtained. The advantage of the single-step approach is its capability to handle both weakly and strongly absorbing aerosols[11]. The drawback is that convergence may not be achieved immediately in some cases, making it difficult to apply the algorithms to large satellite data sets.

The two types of algorithms are fairly complicated. They require, in particular, large look-up tables of aerosol optical properties, aerosol radiance, or top-of-atmosphere radiance. These tables are called internally as the atmospheric correction (standard procedure or non-linear optimization) is effected. The "spectral matching" algorithms require a priori knowledge of the bio-optical model, even though this model can be general and encompass a large variety of water types. Changing the bio-optical model, which may be necessary depending on the region, requires regenerating the top-of-atmosphere radiance.

Other algorithms based on nonlinear regression methods have been developed, using perceptrons[14] or ridge function fields[15-16]. Depending on the selected class of regression models, but generally speaking, the advantage of regression approaches over the aforementioned algorithms is the rapidity of execution. Basically, the inverse model is first adjusted on a statistically significant synthetic data set, and applied next to actual data. However, because distributions of synthetic and actual data may differ from each other, due to radiometric calibration errors and radiation-transfer modeling uncertainties, the efficiency of regression techniques is strongly influenced by the overall noise distribution. Furthermore, like in the "spectral matching" algorithms, the adjustment is made using a specified bio-optical model, which may not represent the range of expected oceanic regimes.

It may be possible, however, to combine linearly the top-of-atmosphere radiance in selected spectral bands, so that the atmosphere and surface effects are reduced substantially. This approach has been proposed to estimate chlorophyll-a concentration directly[17]. The method requires appropriate modeling or decomposition of the perturbing effects and sufficient sensitivity of the linear combination to pigment concentration. One advantage is that the bio-optical model can be changed easily, depending on the biological province considered. Another advantage is that the method is fast in application, and the resulting product is less noisy. Importantly, explicit knowledge of aerosol optical properties is avoided. The method can also be extended to estimate the marine signal directly, without any assumption about the bio-optical properties of the water body, the subject of the present study. First, we describe the approach and the procedure to determine the coefficients of suitable linear combinations, and we evaluate the impact of residual atmospheric effects on the retrieval of the marine signal. Finally we debate the advantages and drawbacks of the algorithm, and we conclude with a discussion of improvements and potential developments.

2. METHODOLOGY

Instead of using radiance L, we use reflectance R defined as $R = \pi L/F_0 \cos\theta_0$, where F_0 is the extraterrestrial solar irradiance and θ_0 is the solar zenith angle. Neglecting the influence of direct sun glitter, whitecaps, and gaseous absorption, the remaining top-of-atmosphere reflectance $R^*(\lambda)$ at wavelength λ can be expressed as

$$R^*(\lambda) = R_m(\lambda) + R_a(\lambda) + R_{ma}(\lambda) + T_m(\lambda)T_a(\lambda)R_w(\lambda), \quad (1)$$

where $R_m(\lambda)$ and $R_a(\lambda)$ are the pure molecule- and aerosol-scattering contributions, respectively, $R_{ma}(\lambda)$ is the effect of molecule-aerosol interaction, $R_w(\lambda)$ is the water-body reflectance, and $T_m(\lambda)$ and $T_a(\lambda)$ are diffuse transmittances due to molecules and aerosols, respectively.

The molecular reflectance $R_m(\lambda)$ can be computed precisely from atmospheric pressure and wind speed. One can therefore subtract $R_m(\lambda)$ from $R^*(\lambda)$ in Equation (1) to form

$$R_c = R^*(\lambda) - R_m(\lambda) = R_a(\lambda) + R_{ma}(\lambda) + T_m(\lambda)T_a(\lambda)R_w(\lambda) = R'(\lambda) + T_m(\lambda)T_a(\lambda)R_w(\lambda). \quad (2)$$

In this expression, the effect of aerosols is essentially confined to $R'(\lambda)$. The transmittance $T_a(\lambda)$ is generally close to 1 and varies by a few percent.

Linearly combining the corrected reflectance in spectral bands centered at λ_i yields the following index

$$I = \sum_i [a_i R'(\lambda_i)] + \sum_i [a_i T_m(\lambda_i)T_a(\lambda_i)R_w(\lambda_i)]. \quad (3)$$

To eliminate most of the atmospheric influence on I, one has to find coefficients a_i that verify

$$\sum_i [a_i R'(\lambda_i)] = 0. \quad (4)$$

For this, $R'(\lambda_i)$ is decomposed in principal components[18], i.e.,

$$R'(\lambda_i) = \sum_j [b_j e_{ji}], \quad (5)$$

where e_j are the eigenvectors of the decomposition, e_{ji} their components, and b_j the associated coefficients. In general, a satisfactory representation can be obtained with only a few eigenvectors, since R' is a smooth function of wavelength. Substituting R' by its expression, Equation (4) becomes

$$\sum_i \{a_i \sum_j [b_j e_{ji}]\} = \sum_j \{b_j \sum_j [a_i e_{ji}]\} = 0. \quad (6)$$

To satisfy Equation (6), it is sufficient to have for each e_j

$$\sum_i [a_i e_{ji}] = 0. \quad (7)$$

This system of linear equations is undefined, which in some way offers a lot of flexibility. It can be solved using p wavelengths and $n = p-1$ eigenvectors, and $a_1 = 1$, assuming that the last eigenvector of the $R'(\lambda_i)$ decomposition can be neglected (see below). Note that the coefficients b_j, which vary with geometry and geophysical conditions (i.e., are different for each pixel), do not need to be known.

Table 1 summarizes the principal component analysis of 55,000 $R'(\lambda_i)$ vectors generated for a wide range of realistic atmosphere, surface, chlorophyll-a concentration (Case 1 waters), and angular conditions, and gives the resulting a_i coefficients. The selected wavelengths are the central wavelengths of the Sea-viewing Wide Field-of-view Sensor (SeaWiFS) spectral bands, i.e., 412, 443, 490, 510, 555, 670, 765, and 865 nm (hereafter also referred to as 1, 2, ..., 8). The view and sun zenith angles ranged between 0 and 60 degrees, the relative azimuth angle from 0 to 180 degrees, the

aerosol optical thickness at 550 nm between 0.01 and 0.8, the wind speed between 0 and 15 ms^{-1}, and the surface pressure from 1003 to 1023 hPa. Mixtures of continental and maritime aerosols, urban and maritime aerosols, and continental and urban aerosols were considered, as well as biomass burning and dust aerosols. Cases for which the sun glint reflectance was above 0.04 were discarded. The radiation-transfer code of Vermote et al.[19], which takes properly into account molecule-aerosol interaction and surface-atmosphere coupling, was used to simulate $R'(\lambda_i)$. Six sets of three wavelengths were analyzed, starting with the longest three wavelengths, and then progressing towards shorter wavelengths by substituting the longest wavelength by a shorter wavelength. For each set of wavelengths, two eigenvectors are generally sufficient to represent R', since they explain above 99.999% of the variance in the data sets.

Table 1. Principal component analysis of 55,000 ***R'*** vectors generated for a wide range of realistic atmosphere, surface, chlorophyll concentration (Case 1 waters) and angular geometry conditions, and resulting ***a*** vectors.

. Wavelengths: 670, 765, 865 nm *. Eigenvector matrix:* . 0.995750, 0.999984, 0.996156 . 0*.0920276, -0.00439613, -0.0875771* *. -0.00188663, 0.00405639, -0.00218612* *. Variances: 0.994606, 0.00538605, 8.26426e-06* ***a** = [1.0, -2.13831, 1.14699]*	*. Wavelengths 490, 510, 555 nm* *. Eigenvector matrix:* *. 0.998446, 0.999934, 0.997791* *. 0.0556427, 0.0107102, -0.0664124* *. -0.00312565, 0.00493933, -0.00182223* *. Variances: 0.997447, 0.00254047, 1.24957e-05* ***a** = [1.0, -1.58025, 0.582993]*
. Wavelengths: 555, 670, 765 nm *. Eigenvector matrix:* *. 0.993376, 0.999702, 0.994661* *. 0.114572, -0.0118909, -0.102473* *. -0.00886386, 0.0211049, -0.0123594* *. Variances: 0.991851, 0.00792292, 0.000225579* ***a** = [1.0, -2.38100, 1.39436]*	*. Wavelengths: 443, 490, 510 nm* *. Eigenvector matrix:* *. 0.995186, 0.999645, 0.997447* *. 0.0979817, -0.0263064, -0.0713952* *. 0.00106371, -0.00397815, 0.00292562* *. Variances: 0.994861, 0.00512990, 8.50544e-06* ***a** = [1.0, -3.73988, 2.75039]*
. Wavelengths: 510, 555, 670 nm *. Eigenvector matrix:* *. 0.995636 0.999780 0.993781* *. 0.0930926 0.0178654 -0.111240* *. -0.00696114 0.0109714 -0.00406350* *. Variances: 0.992818, 0.00711989, 6.17803e-05* ***a** = [1.0, -1.57609, 0.583740]*	*. Wavelengths: 412, 443, 490 nm* *. Eigenvector matrix:* *. 0.991206, 0.999972, 0.991766* *. 0.132294, -0.00416542, -0.128020* *. -0.00290505, 0.00605232, -0.00319898* *. Variances: 0.988679, 0.0113027, 1.84345e-05* ***a** = [1.0, -2.08338, 1.10118]*

Using the results of Table 1, the retrieval of the marine signal, i.e., $T_m(\lambda_i)T_a(\lambda_i)R_w(\lambda_i)$, is effected as follows. First, the marine signal in spectral band 6 is estimated by combining linearly the corrected reflectance $R_c(\lambda_i)$ in spectral bands 6, 7, and 8. Since the marine reflectance in spectral bands 7 and 8 is practically zero for the waters considered (Case 1), the linear combination gives the marine signal directly. Second, the marine signal in spectral band 5 is estimated by combining linearly the corrected reflectance in spectral bands 5, 6, and 7. In this case, the marine signal in band 6 (not null), estimated in the previous step, is subtracted from the linear combination of corrected reflectance. Next, the scheme proceeds in the same way to estimate the marine signal at shorter wavelengths. In the last step, the marine signal in

spectral band 1 is estimated by combining linearly the corrected reflectance in bands 1, 2, and 3, and by subtracting the marine signal in bands 2 and 3 estimated in the previous steps. Thus, assuming that the water-body reflectance is null in the two longest wavelengths (Case 1 waters), the marine signal at the first 6 wavelengths is obtained using the following equations

1: $T_m(\lambda_6)T_a(\lambda_6)R_w(\lambda_6) \approx \sum_i [a_i R_c(\lambda_i)]$, $i = 6, 7, 8$

2: $T_m(\lambda_5)T_a(\lambda_5)R_w(\lambda_5) \approx - a_6 T_m(\lambda_6)T_a(\lambda_6)R_w(\lambda_6) + \sum_i [a_i R_c(\lambda_i)]$, $i = 5, 6, 7$

.

.

.

6: $T_m(\lambda_1)T_a(\lambda_1)R_w(\lambda) \approx - a_2 T_m(\lambda_2)T_a(\lambda_2)R_w(\lambda_2) - a_3 T_m(\lambda_3)T_a(\lambda_3)R_w(\lambda_3) + \sum_i [a_i R_c(\lambda_i)]$, $i = 1, 2, 3$ (8)

Note that the method is also applicable to optically complex waters that are reflecting in the near infrared (Case 2), but in this case longer wavelengths (e.g., 1040 and 1600 nm) need to be considered in the algorithm. One potential drawback of using longer wavelengths, however, is that error propagation to the shorter wavelengths might be larger. For Case 2 waters, however, estimation of sediment and chlorophyll-a concentrations might not require observations in the blue.

3. RESULTS

Figures 1 and 2 display the residual atmospheric and surface effects, i.e., $\sum_i [a_i R'(\lambda_i)]$, as a function of aerosol optical thickness at 550 nm for the 6 sets of wavelengths. All the 55,000 cases are plotted in Figure 1, and the average error and standard deviation in bins of 0.1 in aerosol optical thickness are given in Figure 2. The residual errors are generally small compared with the marine signal to retrieve, except at large optical thickness. The global standard deviations are 0.0006 (670 nm), 0.0021(555 nm), 0.0008 (510 nm), 0.0004 (490 nm), 0.0010 (443 nm), and 0.0010 (412 nm). When the aerosol optical thickness is less than 0.3 (i.e., values mostly encountered over the ocean), the standard deviations are reduced to 0.0004, 0.0010, 0.0005, 0.0002, 0.0004, and 0.0005, respectively. The residual errors exhibit a negative bias that increases in magnitude with increasing aerosol optical thickness. For some wavelengths, the dependence with optical thickness is nonlinear. The effect is especially pronounced at 555 and 412 nm. One way to reduce the bias is to take into account the last (least significant) eigenvector of the decomposition in principal components. In this case, the average value of the associated coefficient is used. Unfortunately, this procedure reduces the bias globally, i.e., the magnitude of the bias may be increased a low aerosol optical thickness. Another way to reduce the bias is to confine the analysis to probable cases, or to take into account the statistics of variability of the geophysical parameters that affect R' in the construction of the synthetic data set (instead of giving equal weight to all possible values).

The resulting errors on the retrieval of the marine signal, i.e., $T_m(\lambda_i)T_a(\lambda_i)R_w(\lambda_i)$, $i = 1, 2, ..., 6$, are displayed in Figures 3 and 4 when the aerosol optical thickness at 550 nm is between 0.1 and 0.2. All the cases are plotted in Figure 3, and the average error and standard deviation in bins of marine signal (10 bins over the range of variability of the marine signal) are displayed in Figure 4. As expected, the errors increase with decreasing wavelength, due to propagation of the residual atmospheric and surface effects. Estimated and actual values agree at wavelengths below 443 nm. At 443 and 412 nm, the correlation between estimated and actual values remains strong, but the estimated values are significantly biased. More precisely, the mean difference is -0.0004 at 670 nm, -0.0008 at 555 nm, -0.0015 at 510 nm, 0.0021 at 490 nm, -0.0043 at 443 nm, and -0.0083 at 412 nm.

Figure 5 summarizes the performance statistics for the retrieval of the marine signal. Bias and standard deviation are displayed as a function of aerosol optical thickness at 550 nm. The performance is quickly degraded as aerosol optical thickness increases, and become unacceptable when the optical thickness is above 0.3 (e.g., standard deviations above 0.006 and 0.008 at 443 and 412 nm, respectively). Situations of large aerosol optical thickness, however, are usually not encountered in the open ocean[20], but they occur during dust or biomass burning events and pollution outbreaks.

4. CONCLUSIONS

Combining linearly satellite reflectance corrected for molecular scattering and sun glint contributions allows one to reduce substantially the influence of the atmosphere and surface in satellite ocean-color imagery. The perturbing effects on the marine signal are minimized adequately for each set of wavelengths, except when aerosol loading is large. The residual effects, however, exhibit a negative bias that increases with increasing aerosol optical thickness. The bias can be globally reduced, by taking into account all the eigenvectors of the decomposition in principal components (instead of the most significant ones). This procedure, however, may increase the bias at low to moderate optical thickness, i.e., for situations mostly encountered over the ocean. Reduction of the bias could also be achieved by generating the synthetic data set in view of the statistical distribution of the parameters that govern the satellite reflectance.

The resulting errors in the retrieved ocean signal become larger as wavelength decreases, due to propagation from longer wavelengths of the residual effects on the linear combinations of corrected reflectance, which do not minimize completely the influence of the atmosphere and surface. They increase with increasing aerosol optical thickness, becoming unacceptable when the aerosol optical thickness at 550 nm is above 0.3. Performance can be improved, however, by optimizing the set of selected wavelengths, or by using an estimate of the aerosol optical thickness, which can be estimated from the satellite data (precise knowledge of the aerosol optical thickness is not necessary). In any case, the aerosol optical thickness needs to be estimated to correct the ocean signal for aerosol transmittance and deduce the marine reflectance.

One advantage of the method, compared with other techniques, is that no look-up tables of geometry dependent aerosol optical properties or top-of atmosphere reflectance need to be called and, therefore, created. Also, the coefficients of the linear combinations are independent of sun and view angles. Another advantage is the rapid execution of the algorithm. In current “spectral matching” techniques, it is time consuming to find the proper aerosol model or iterate and minimize the difference between simulations and measurements. Importantly, unlike “spectral matching” or nonlinear regression techniques, the method does not require a priori knowledge of the bio-optical model or any assumption about the water body. The method was developed for Case 1 waters, for which the reflectance in the near infrared is practically negligible. It could be extended to Case 2 waters, but this would require selecting longer wavelengths (above 1000 nm), for which Case 2 waters are black, to initiate the algorithm. This possibility and the potential improvements mentioned above are currently under investigation.

ACKNOWLEDGMENTS

This work was supported by the National Aeronautics and Space Administration under Grant # NNG05GR20G, and by the National Science Foundation under Grant # OCE-0417748. The authors wish to thank J. McPherson from the Scripps Institution of Oceanography, University of California San Diego for technical help.

REFERENCES

1. Gordon, H. R., "Removal of atmospheric effects from satellite imagery of the oceans", *Appl. Opt*., **17**, pp. 1631-1636, 1978.
2. Viollier, M., D. Tanré, and P.-Y. Deschamps, "An algorithm for remote sensing of water color from space", *Boundary-Layer Meteor*., **18**, pp. 247-267, 1980.
3. Gordon, H. R., and M. Wang, 1994, "Retrieval of water-leaving radiance and aerosol optical thickness over the oceans with SeaWiFS: a preliminary algorithm", *Appl. Opt.*, **33**, pp. 443-452, 1994.
4. Gordon, H. R., "Atmospheric correction of ocean color imagery in the Earth Observing System era", *J. Geophys. Res*., **102**, pp. 17107-17118, 1997.
5. Fukushima, H., A. Higurashi, Y. Mitomi, T. Nakajima, T. Noguchi, T. Tanaka, and M. Toratani, "Correction of atmospheric effects on ADEOS/OCTS ocean color data: Algorithm description and evaluation of its performance", *J. Oceanogr.*, **54**, pp. 417-430, 1998.
6. Antoine, D., and A. Morel, "A multiple scattering algorithm for atmospheric correction of remotely sensed ocean colour (MERIS instrument): principle and implementation for atmospheres carrying various aerosols including absorbing ones", *Int. J. Remote Sens.*, **20**, pp. 1875-1916.
7. Gao, B.-C., M. J. Montes, Z. Ahmad, and C. O. Davis, "Atmospheric correction algorithm for hyper-spectral remote sensing of ocean color from space", *Appl. Opt.*, **39**, pp. 887-896, 2000.
8. J.-M. André and A. Morel, A., "Atmospheric corrections and interpretation of marine radiances in CZCS imagery, revisited", *Oceanol. Acta*, **14**, pp. 3-22, 1991.
9. Land, P. E., and J. D. Haigh, "Atmospheric correction over case 2waters using an iterative fitting algorithm", *Appl. Opt*., **35**, pp. 5443-5451, 1996.
10. Fraser, R. S., S. Mattoo, E.-N Yeh, and C. R. McClain, "Algorithm for atmospheric and glint corrections of satellite measurements of ocean pigment", *J. Geophys. Res*., **102**, pp. 17107-17118, 1997.
11. Gordon, H.R., T. Du, and T. Zhang, Remote sensing of ocean color and aerosol properties: resolving the issue of aerosol absorption, *Appl. Opt.*, **36**, pp. 8670-8684, 1997.
12. Zhao, F., and T. Nakajima, "Simultaneous determination of water reflectance and aerosol optical thickness from Coastal Zone Color Scanner measurements, *Appl. Opt*., **36**, pp. 6949-6956, 1997.
13. Chomko, R., and H.R. Gordon, "Atmospheric correction of ocean color imagery: use of the Junge power-law aerosol size distribution with variable refractive index to handle aerosol absorption", *Appl. Opt.*, **37**, pp. 5560-5572, 1998.
14. Schiller, H., and R. Doerffer, "Neural network for emulation of an inverse model - operational derivation of case II properties from Meris data," *Int. J. Rem. Sen.*, **20**, pp. 1735–1746, 1999.
15. Pelletier, B., and R. Frouin, "Fields of nonlinear regression models for inversion of satellite data," *Geophys. Res. Lett.* **31**, L16304, 2004.
16. Pelletier, B., and R. Frouin, "Remote sensing of phytoplankton chlorophyll-a concentration by use of ridge function fields," *Appl. Opt.*, **45**(4), pp. 794–798, 2006.
17. Frouin, R., P.-Y. Deschamps, L. Gross-Colzy, H. Murakami, and T. Y. Nakajima, "Retrieval of chlorophyll-concentration via linear combination of Global Imager data", *J. Oceanogr.*, **62**, pp. 331-337, 2006.
18. Jollife, I. T., "Principal component analysis", Springer-Verlag, New York, 1986.
19. Vermote, E. F., D. Tanré, J.-L. Deuzé, M. Herman, and J.-J. Morcrette, "Second simulation of the satellite signal in the solar spectrum: An overview", *IEEE Trans. Geosci. Remote Sens*., **35**, pp. 675-686, 1997.

20. Knobelspiesse, K. D., C. Pietras, G. S. Fargion, M. Wang, R. Frouin, M. A. Miller, A. Subramaniam, and W. M. Balch, "Maritime aerosol optical thickness measured by handheld sun photometers", *Rem. Sen. Environ*., **93**, pp. 87-106, 2004.

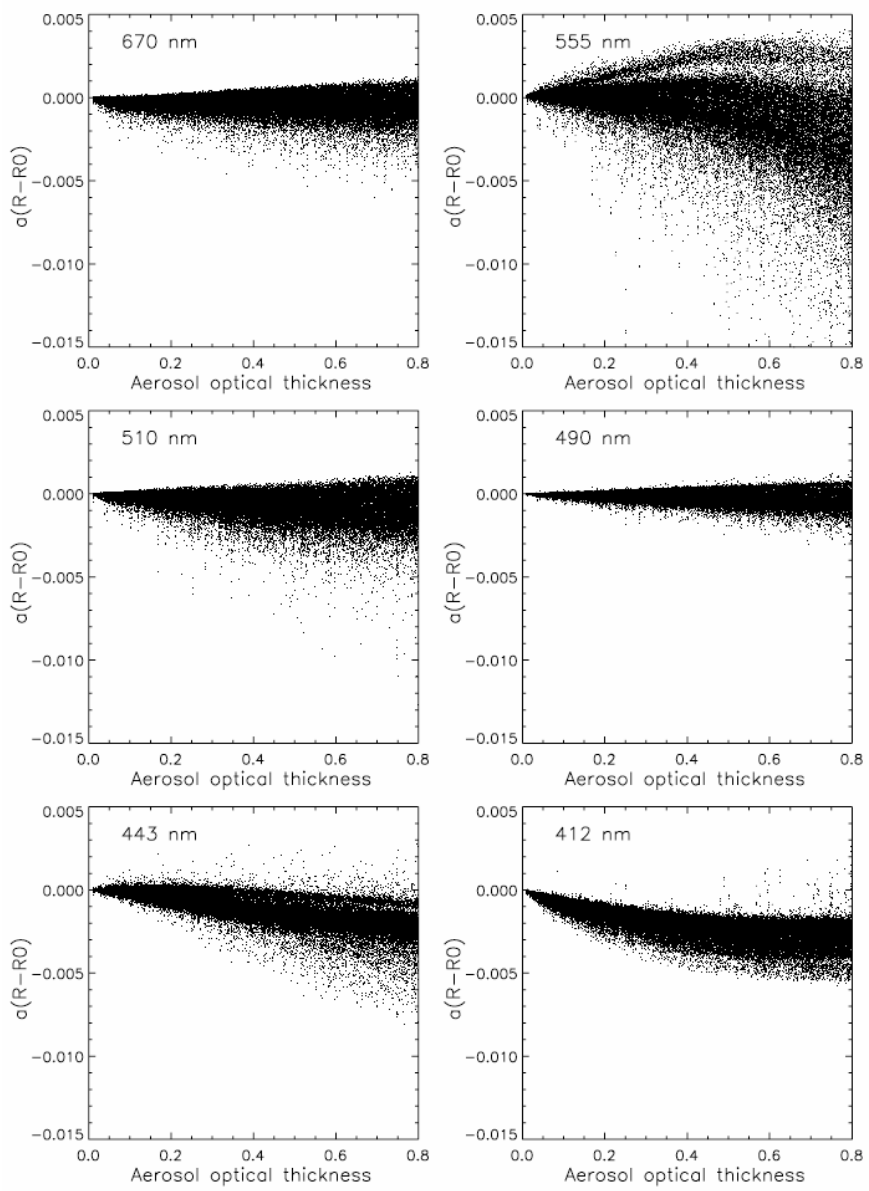

Figure 1. Residual perturbing effects of the atmosphere and surface, i.e., $\sum_i [a_i R'(\lambda_i)]$, as a function of aerosol optical thickness at 555 nm for all (i.e., 55,000) cases.

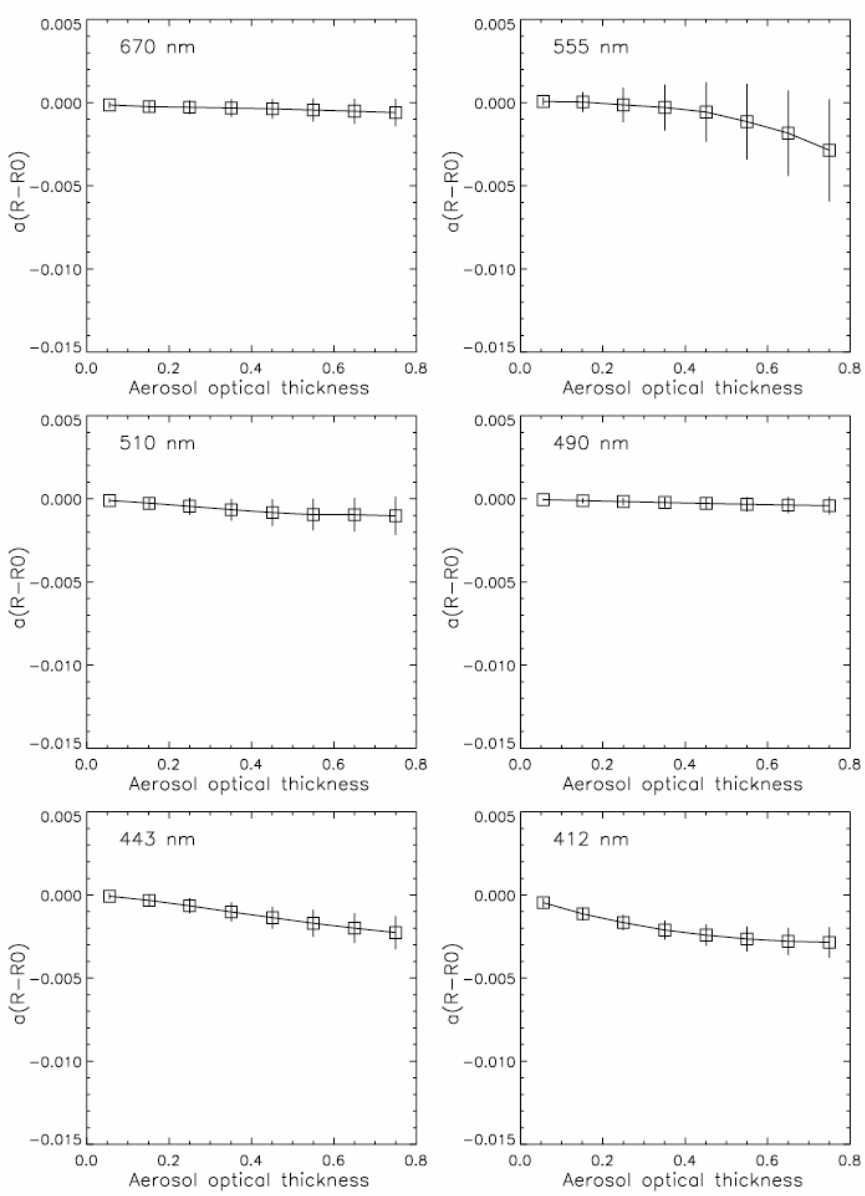

Figure 2. Average and standard deviation of residual perturbing effects, displayed in bins of 0.1 in aerosol optical thickness at 555 nm.

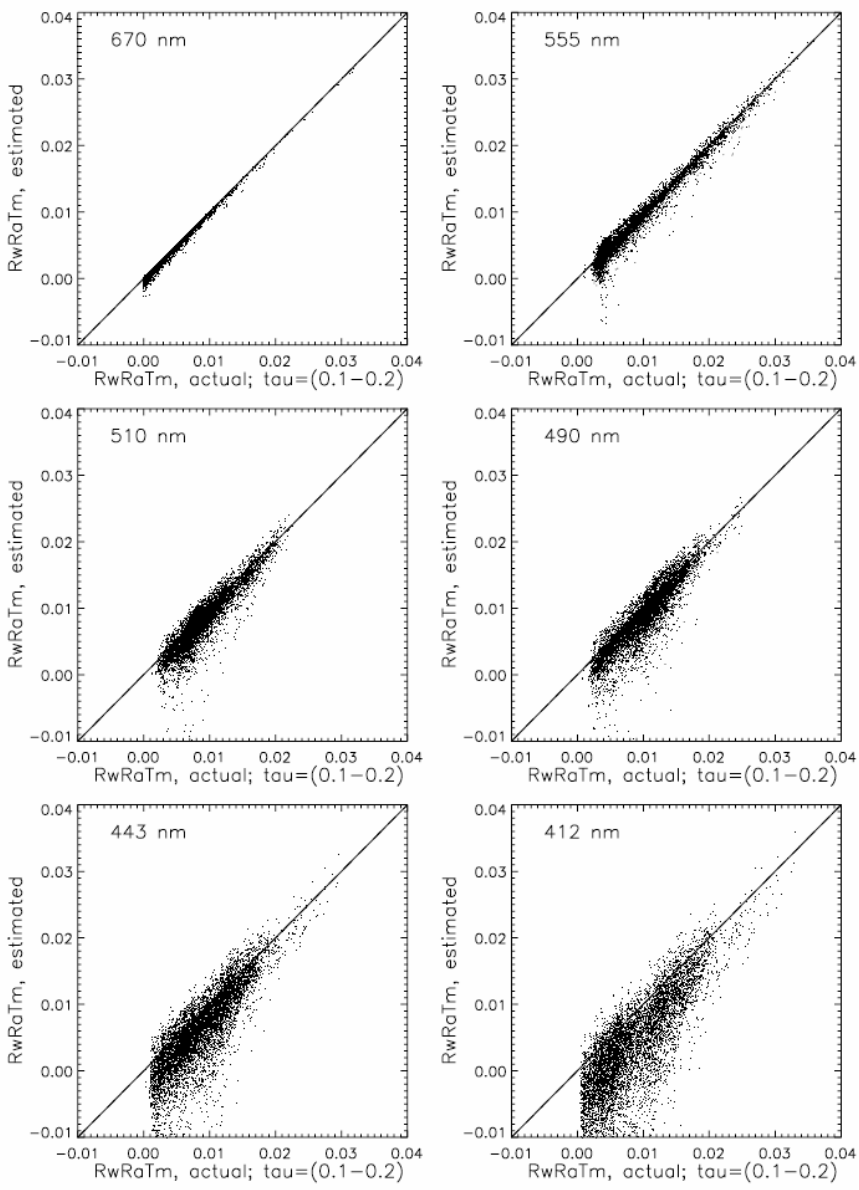

Figure 3. Comparison of estimated and actual ocean signal, i.e., $T_m(\lambda)T_a(\lambda)R_w(\lambda)$, when the optical thickness at 550 nm is between 0.1 and 0.2.

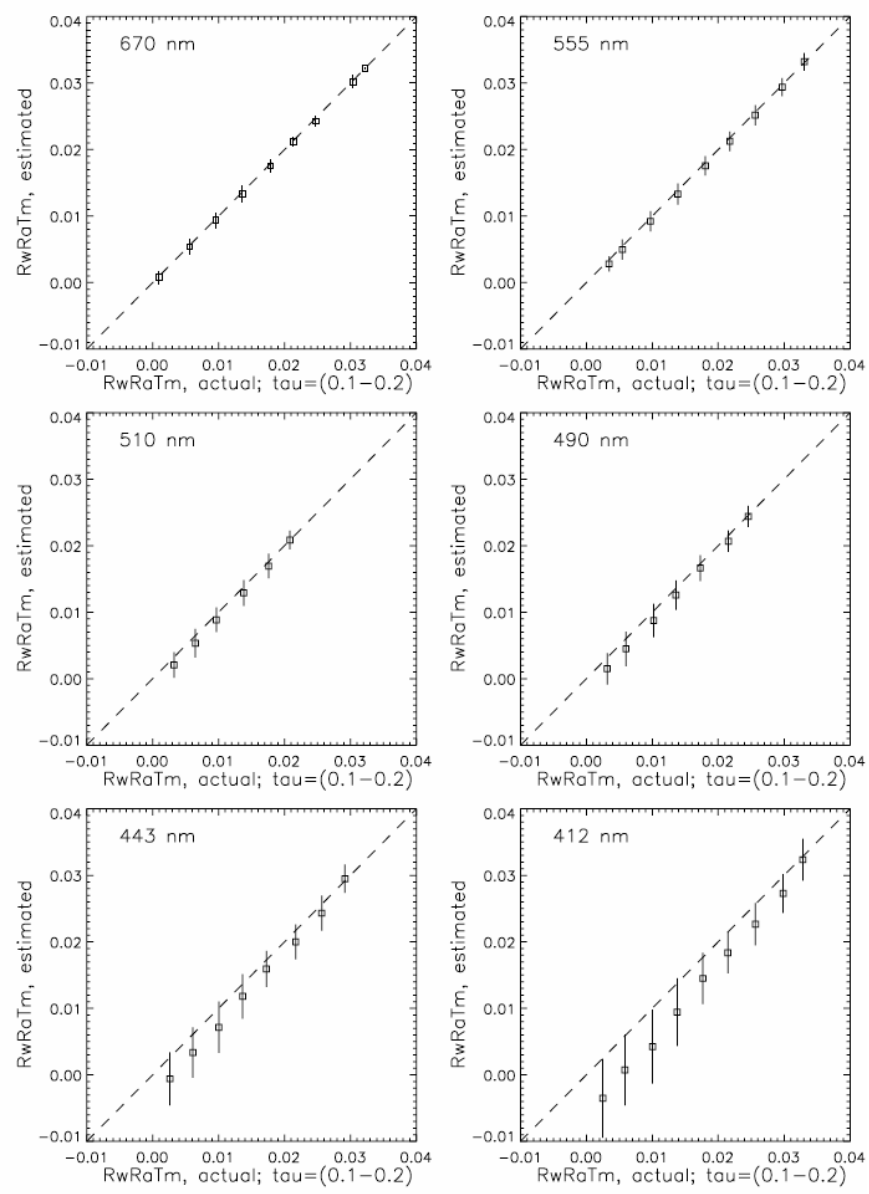

Figure 4. Same as Figure 3, but bias and standard deviation in bins of 0.1 in aerosol optical thickness at 555 nm.

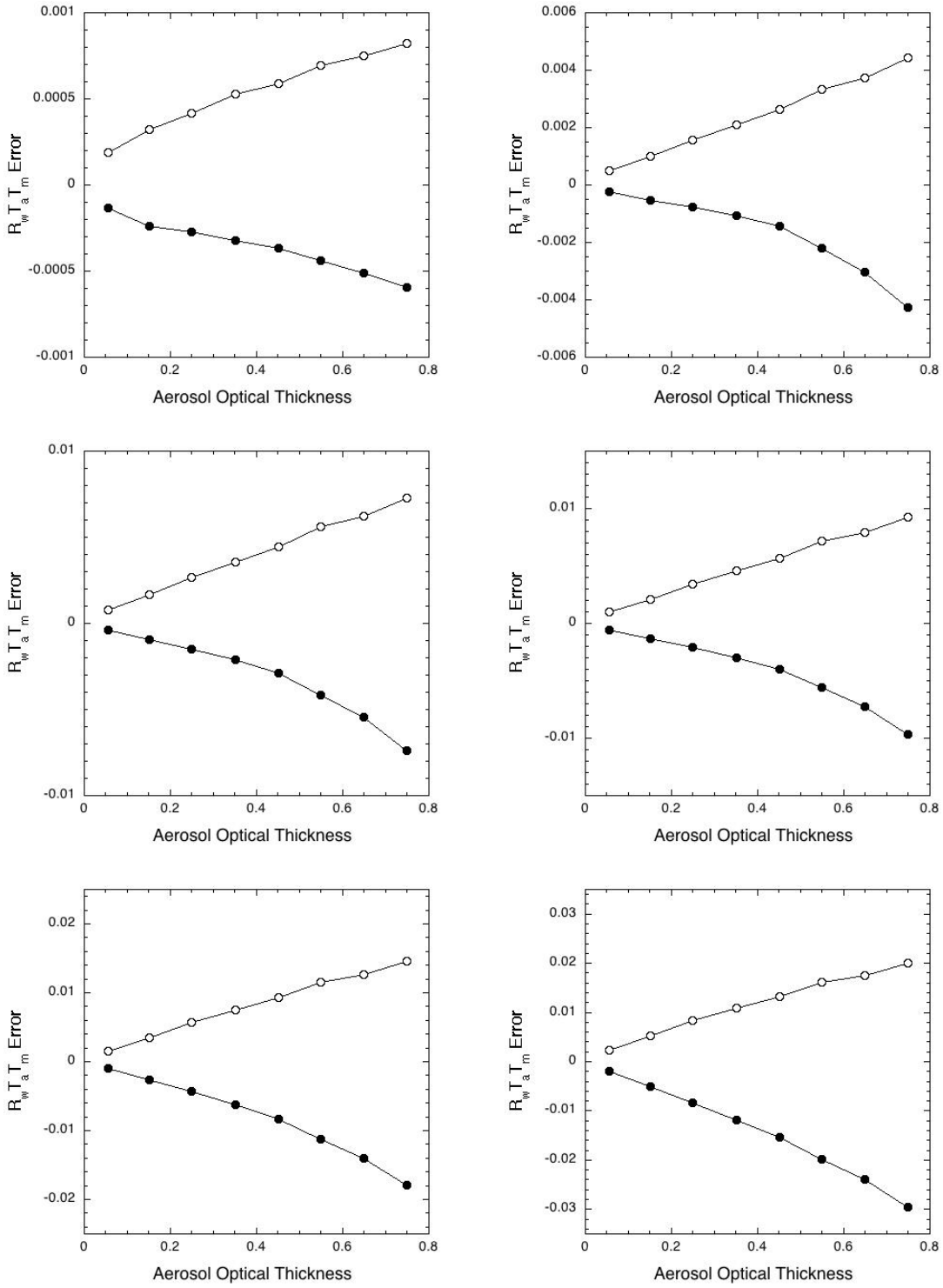

Figure 5. Performance statistics for the retrieval of $T_m(\lambda)T_a(\lambda)R_w(\lambda)$. Bias (solid circles) and standard deviation (open circles) are given as a function of the aerosol optical thickness at 550 nm. Top: 670 and 555 nm; Middle: 510 and 490 nm; and Bottom: 443 and 490 nm.